

Geophysical Research Letters



RESEARCH LETTER

10.1029/2020GL089203

Key Points:

- *PKP* precursor observed at distance beyond 155°
- *D*'' scattering of teleseismic waves at 6 Hz
- Radiative transfer simulation used to locate regions of heterogeneity

Supporting Information:

- Supporting Information S1

Correspondence to:

C. Sens-Schönfelder,
sens-schoenfelder@gfz-potsdam.de

Citation:

Sens-Schönfelder, C., Bataille, K., & Bianchi, M. (2021). High Frequency (6 Hz) *PKPab* precursors and their sensitivity to deep Earth heterogeneity. *Geophysical Research Letters*, 48, e2020GL89203. <https://doi.org/10.1029/2020GL089203>

Received 5 JUN 2020
 Accepted 24 NOV 2020

High-Frequency (6 Hz) *PKPab* Precursors and Their Sensitivity to Deep Earth Heterogeneity

C. Sens-Schönfelder¹ , K. Bataille^{1,2}, and M. Bianchi³ 

¹Seismology Section (2.4), GFZ German Research Centre for Geosciences, Telegrafenberg, Potsdam, Germany, ²Earth Sciences Department, University of Concepción, Concepción, Chile, ³Instituto de Astronomia, Geofísica e Ciências Atmosféricas, Universidade de São Paulo, Sao Paulo, Brazil

Abstract We present observations on a new precursory phase of seismic waves scattered in the deep Earth. This phase arrives prior to the *PKPab* wave at epicentral distances larger than 155°, and we call it *PKPab* precursor. We show that the presence of the *PKPab* precursor is a necessary consequence of scattering in *D*'', which is the commonly accepted cause of the *PKPdf* precursor at distances smaller than 145°. *PKPdf* waves that propagate through the inner core should arrive before the *PKPab* precursor but those, are strongly attenuated in the inner core at frequencies between 4 Hz and 8 Hz used here, making the *PKPab* precursor the earliest teleseismic signal at distances larger than 155°. Calculated *PKPab* precursor sensitivity kernel shows that this phase is mostly sensitive to scattering along the closest *PKPbc* path between source and receiver. It can thus help to constrain the lateral distribution of heterogeneity along *D*''.

Plain Language Summary A new discovered seismic signal recorded far away from earthquakes, by stations on the other side of Earth, will help to study the properties of the core–mantle boundary. We use high frequencies at which seismic waves do not propagate through the Earth's inner core but are instead propagated around it by deflection at heterogeneity located along the core–mantle boundary.

1. Wave Scattering in the Deep Earth

The core–mantle boundary (CMB) is of significant interest for the dynamics of our planet as it controls the heat transfer between core and mantle with consequences for the geodynamo (Labrosse, 2014; Olson, 2016) and plate tectonics. Above the CMB, the 200-km-thick *D*'' layer forms the heterogeneous base of the mantle and hosts the large low shear velocity provinces and the ultra-low-velocity zones (McNamara, 2019; Yu & Garnero, 2018). The *D*'' layer is believed to be the source region of magmatic plumes (Burke et al., 2008; French & Romanowicz, 2015) and the storage area of subducted lithosphere. Resulting chemical heterogeneity together with laterally varying temperature profiles and phase transitions cause significant spatial variability in the elastic properties of the lower mantle. Images of *D*'' have been provided by global seismic tomography studies (Kustowski et al., 2008; Ritsema et al., 2011) while its internal structure is constrained generally using top and bottom reflections as well as transmitted and diffracted wave observations (Euler & Wysession, 2017; Frost & Rost, 2014; Hansen et al., 2020; Shen et al., 2016; Sun et al., 2013; Wang & Wen, 2004). A review of seismic investigations of the lower mantle can be found in Lay and Garnero (2011). Together with geodynamic models, the seismological observations confirm that the lower mantle is a region of increased elastic heterogeneity including length scales below the resolution of seismic tomography (Schuberth et al., 2009) that are associated with scattering of seismic energy.

Investigating Earth with scattered waves is different from ballistic waves. Scattered waves do not propagate along deterministic paths predicted by ray theory but reach the receiver on complicated trajectories that can only be described in a probabilistic sense (Pacheco & Snieder, 2005). Normally, scattered waves travel longer paths and thus arrive after the ballistic waves forming the coda of seismic records (Aki & Chouet, 1975; Gaebler et al., 2015; Obara & Sato, 1995; Sens-Schönfelder et al., 2009). Additionally, since the wave velocity at the core is lower than at the mantle, scattering in the deep Earth can cause seismic energy to arrive both at the coda of a ballistic phase and prior to a ballistic phase as a precursor.

© 2020. The Authors.
 This is an open access article under the terms of the [Creative Commons Attribution](https://creativecommons.org/licenses/by/4.0/) License, which permits use, distribution and reproduction in any medium, provided the original work is properly cited.

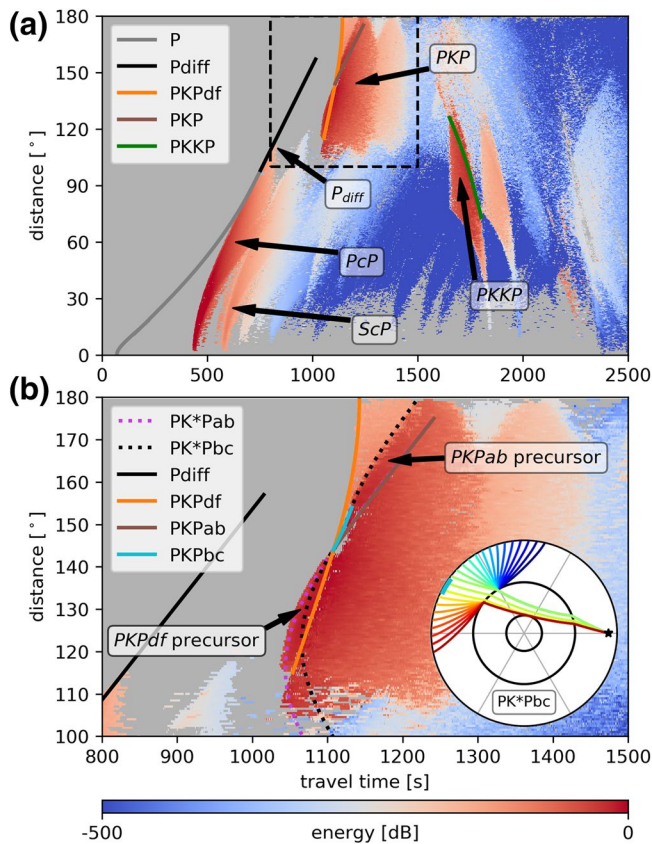


Figure 1. Increase of seismic energy due to scattering in a 50-km-thick layer above the CMB. Simulations used a 600-km-deep P wave source in the velocity and attenuation model ak135-f (Kennett et al., 1995; Montagner & Kennett, 1996). (a) Arrival times of seismic phases and relevant regions of the time–distance domain that have been investigated for scattering in the deep Earth are indicated. (b) A zoom into the time–distance window of PKP waves (dashed box, panel a). Theoretical onset times for waves scattered at the CMB are indicated and labeled with “*” indicating the scattering event. The frequently discussed $PKPdf$ precursor and the $PKPab$ precursor discussed below are labeled. Inset in (b) shows a cross section of the Earth with the paths of the fastest PK^*Pbc waves. CMB and ICB are indicated. The blue bar at the surface shows that distance range of $PKPbc$. CMB, core–mantle boundary; ICB, inner core boundary.

Figure 1 shows the increase of scattered intensity due to a 50-km-thick scattering layer above the CMB calculated with differential radiative transfer simulations as detailed in the supporting information Text S1, which contains additional references to Takeuchi (2016) and Trabant et al. (2012). The random velocity fluctuations in this heterogeneous layer are described by an exponential autocorrelation function with fluctuation strength of 10% and a correlation length of 0.1 km. A number of time–distance windows of the global wavefield that have been investigated for waves scattered in the deep Earth are shown in Figure 1(a). ScP and PcP top side reflections at the CMB can show precursors that originate by reflections above the CMB as well as coda waves from reverberations in the heterogeneous layer or off great-circle reflections (Gassner et al., 2015; Shen et al., 2016; Wu et al., 2014). Short distance $PKKP$ precursors (Chang & Cleary, 1978, 1981; Earle & Shearer, 1997) also originate from off great-circle bottom side reflections at the CMB (cf., Figure 1(a)). PKP precursors probe the D'' layer in near-vertical transmission.

Paths corresponding to the PK^*Pbc onset are shown in the inset of Figure 1(b). Figure S1 shows paths and corresponding onset times for source and receiver side D'' scattering of the $PKPab$ and $PKPbc$ branches. Scattering of PKP waves at D'' can divert energy into the distance range below 145° which would otherwise not be accessible to PKP (Haddon & Cleary, 1974; Hedlin et al., 1997). These waves form the $PKPdf$ precursor which arrives before the $PKPdf$ phase (cf., Figure S1(e)) that travels through the inner core ($PKIKP$) and is the earliest ballistic phase in the core shadow. This situation provides exceptional conditions for the observation of $PKPdf$ precursors (cf., Figure 1(b)). Opportunities to probe the lower mantle by transmission in a near-horizontal direction are provided by P_{diff} coda (cf., Figure 1). While diffraction along the CMB vanishes with increasing frequency, at short period, P_{diff} coda waves in the core shadow zone have been interpreted as a sign of scattering along the CMB (Bataille & Lund, 1996) or, as a signature of scattering throughout the mantle (Earle & Shearer, 2001). An overview of the travel time–distance windows in which scattered waves from the deep Earth can be observed is given in Shearer (2015).

The time window between $PKPdf$ and $PKPab$ at distances beyond the $PKPbc$ window ($\Delta > 155^\circ$) has rarely been investigated for the arrival of scattered energy as it is affected by the coda of $PKPdf$ which can be generated locally in the crust below the receiver. Still, arrivals in a continuation of $PKPbc$ at the c-cusp have been identified by Nakanishi (1990), Tanaka (2005), and Zou et al. (2008) and have been interpreted as com-

pressional waves diffracted along the inner core boundary (ICB). While ICB diffraction is a likely scenario at low frequencies, Nakanishi (1990) and Tanaka (2005) note that CMB scattering might become important at higher frequencies. Adam and Romanowicz (2015) reported the arrival of a 0.5–2-Hz scattered signal in the same time–distance window and interpreted it as energy being scattered at the ICB.

Understanding the origin of such faint signals arriving from the deep Earth provides a powerful tool to investigate the small-scale structure of the deep mantle in terms of its statistical properties, that is, the strength of elastic parameter fluctuations and their size distribution. It can yield valuable information about the distribution of chemical or thermal heterogeneity without the blurring effect of the tomographic filter. It also may help to constrain the depth extent and lateral distribution of features like plume clusters (McNamara, 2019) or accumulations of heterogeneous material in the basal mélange formed from subducted slabs (Tackley, 2012).

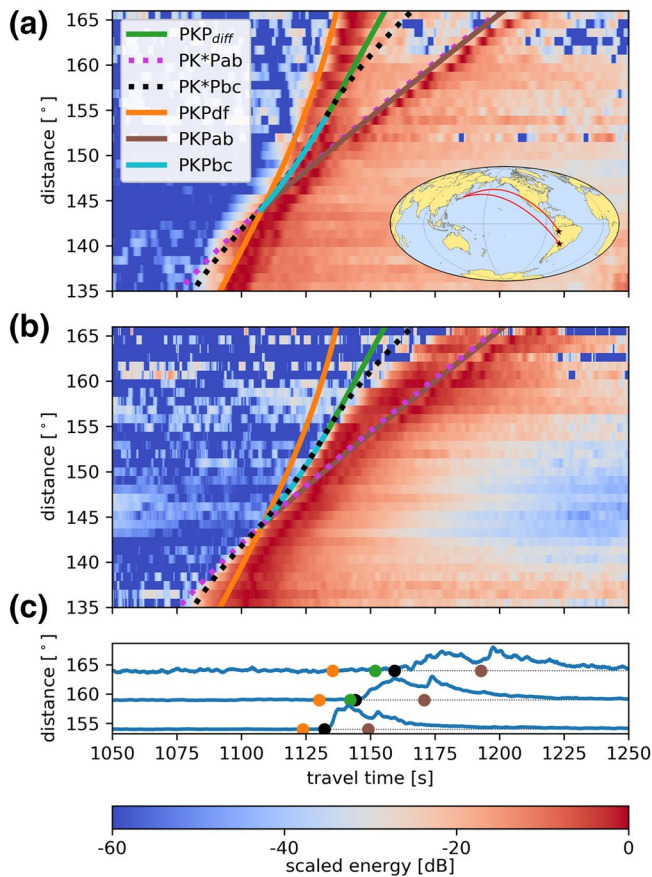


Figure 2. Composite image of stacked seismogram envelopes from Argentina and Peru deep earthquakes recorded in Japan. Arrival times of ballistic and scattered core phases are indicated. Panels (a) and (b) show the 0.35–0.7 Hz and 4–8 Hz frequency bands, respectively. The logarithmic color scale is scaled between maximum and noise level for the individual distance bins. Inset shows the great circle between epicenters (stars) and recording stations. (c) Displays selected seismogram envelopes from panel (b) with dots indicating the arrival times of the ballistic phases and the onset time of *PK*Pbc* with colors corresponding to the legend in (a). See Figures S2 and S3 for envelopes at more distances.

propagating through the inner core in the 4–8 Hz band. (b) The *PKPdf* phase is strongly attenuated on the path from Peru to Japan at these high frequencies compared to the *PKPab* phase. There is no indication of energy arriving prior to the *PKPdf* below 145°—the known *PKPdf* precursor. Figures 2(b) and 2(c) and Figures S2 and S3 (supporting information) show the same data filtered in the 4–8 Hz frequency band and differ significantly from the low-frequency panel. Three main observations can be made. (a) A significant amount of energy travels through the entire Earth in the 4–8 Hz band. (b) The *PKPdf* phase is strongly attenuated on the path from Peru to Japan at these high frequencies compared to the *PKPab* phase. There is no indication of energy propagating through the inner core in the 4–8 Hz band. (c) For distances $\Delta > 155^\circ$, a distinct increase of energy follows the *PK*Pbc* line of the earliest possible arrival of *D''* scattered *PKPbc* energy in Figure 2(b). This is the *PKPab* precursor that is predicted by the simulations in Figure 1. The slowness of the *PKPab* precursor, derived from the onset of arriving energy, transitions from the slowness of the *PKPbc* phase at the c-cusp ($\Delta = 155^\circ$) to a slowness close to that of *PKPab* for $\Delta > 165^\circ$. This curvature of the hodochron is diagnostic for the origin of the *PKPab* precursor. For increasing distances, the onset of energy is significantly delayed with respect to the arrival time of the inner core-diffracted wave *PKP* – *C_{diff}*. The *PKPdf* precursor for $\Delta < 145^\circ$ follows the *PK*Pab* and *PK*Pbc* lines at $\Delta < 145^\circ$.

We would like to emphasize that the presence of the *PKPab* precursor is not due to a local effect at the source of the event (Argentina) or local disturbances within the HiNet. Figure 3 shows the stacked envelopes of the May 30, 2015 deep Bonin Islands earthquake (Mw 7.8, depth 677 km) recorded at stations from part of the Brazilian Seismographic Network (Bianchi et al., 2018), network codes BL and BR. A clear signal of the *PKPab* precursor following the *PK*Pbc* arrival time is observed for this wave path, too.

2. Observation of the *PKPab* Precursors

Additionally to the *PKPdf* precursor at $\Delta < 145^\circ$, Figure 1(b) shows a further arrival of scattered energy at distances $\Delta > 155^\circ$. For reasons discussed later, we term this phase *PKPab* precursor. This phase has been discussed sporadically in the literature, and there is no consensus about its origin. Waves propagating through the inner core arrive earlier in this distance range, and it is not clear whether the scattered energy that arrives between the *PKPdf* and *PKPab* should be regarded as a coda of *PKPdf* or as a precursory signal to *PKPab*. In contrast to the *PKPdf* precursor at $\Delta < 145^\circ$, the *PKPab* precursor at $\Delta > 155^\circ$ in Figure 1 might thus be hidden in the *PKPdf* coda depending on the relative strength of both signals at the given frequency.

A possibility to observe the *PKPab* precursor unambiguously is to show its spatial coherency over an extended distance range. To avoid the effect of source-side crustal scattering, we use large deep earthquakes. Since lateral variability of *D''* scattering could disturb the spatial coherency when records from different areas are combined, we try to use records from compact regions. Deep sources in South America recorded by the dense Japanese HiNet seismic stations (NIED, 2019; Obara et al., 2005; Okada et al., 2004) offer a perfect source–receiver configuration to observe the desired signals.

Figure 2 shows HiNet vertical seismogram envelopes from two events stacked in 1° distance bins. The first is a 570-km-deep event with Mw 6.8 from January 1, 2011, in Argentina that covers $151^\circ < \Delta < 167^\circ$ while the 592-km-deep Mw 7.5 Peru event from November 24, 2015, covers $135^\circ < \Delta < 152^\circ$. Data processing for Figure 2 is described in the supporting information Text S2. Two frequency bands are shown in Figure 2. The low-frequency band between 0.35 Hz and 0.7 Hz shows energetic arrivals following the *PKPdf* and *PKPab* travel time curves and some energy arriving prior to the *PKPdf* below 145°—the known *PKPdf* precursor. Figures 2(b) and 2(c) and Figures S2 and S3 (supporting information) show the same data filtered in the 4–8 Hz frequency band and differ significantly from the low-frequency panel.

Three main observations can be made. (a) A significant amount of energy travels through the entire Earth in the 4–8 Hz band. (b) The *PKPdf* phase is strongly attenuated on the path from Peru to Japan at these high frequencies compared to the *PKPab* phase. There is no indication of energy

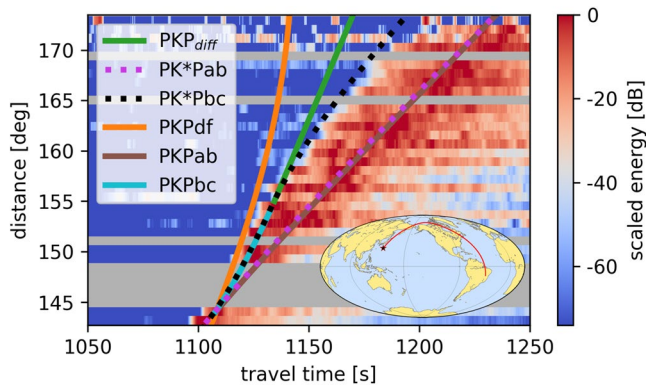


Figure 3. Stacked seismogram envelopes from the Bonin deep earthquakes recorded in Brazil. Arrival times of ballistic and scattered core phases are indicated. Gray intervals represent gaps in the distance coverage of the network. The logarithmic color scale is scaled as in Figure 2. Inset shows the great circle between epicenter (star) and station network.

3. Origin of the *PKPab* Precursor

The onset of *PKPab* precursor emerges at the c-cusp of the hodochron that connects the *PKPbc* and *PKiKP* (inner core reflection) branches with a common slowness. Thus, it seems reasonable to assume a relation of the *PKPab* precursor to one of these two phases. Possible mechanisms could be (a) diffraction of *PKiKP* waves along the ICB or the propagation through a heterogeneous waveguide above the ICB, or (b) deviation of *PKPbc* waves into the shadow of the inner core by scattering in the mantle or outer core. Feasibility to differentiate between these two possibilities is provided by the slowness–distance relation of the earliest energy arrival. For mechanism (a), the energy diffracted along the ICB or propagated around the inner core by any other process that perturbs the ray parameter close to the ICB should arrive with constant slowness for all distances. This should be the slowness of *PKiKP* waves at the c-cusp or a somewhat higher or lower but constant slowness if a low-velocity layer is invoked at the ICB or the head wave propagates with the inner core velocity (*PKPdiff* travel time in Figure 2). Observations in Figures 2(b) and 3 do not favor the ICB-diffraction mechanism (a).

Mechanism (b), that is, the deviation of *PKPbc* wave direction, would mean that part of the *PKPbc* wave energy that travels just atop the inner core gets scattered on its path through the Earth. Depending on the depth distribution of the heterogeneity that causes the scattering, different onset times are possible. However, from the *PKPdf* precursor at distances $\Delta < 145^\circ$, it is known that especially the D'' layer above the CMB scatters wave energy and is thus a right candidate.

As shown in Figure S1, a deviation of the propagation direction of *PKP* waves at the CMB on the source (or receiver) side to create *P*KP* (*PK*P*) waves explains the onset time of the *PKPdf* precursor energy for $\Delta < 145^\circ$ (Figure 2). Scattering of both the *PKPab* and *PKPbc* branches contributes to the *PKPdf* precursor. Source and receiver side scattering of core phases at D'' have very similar effects and we will not differentiate between those in the following.

At distances $\Delta > 155^\circ$, there is no ballistic *PKPbc* arrival and scattered *PK*Pab* energy arrives after the ballistic *PKPab*. However, energy can be shed into this distance range by deviating *PKPbc* energy at D'' . This energy arrives after the *PKPdf* phase, but prior to *PKPab*—the reason for calling it *PKPab* precursor. We emphasize that the predicted onset of *PK*Pbc* is curved, transitioning from the *PKPbc* slowness at short distances, to a higher slowness that is similar to the *PKPab* slowness, at larger distances, just as it is observed in Figures 2(b) and 3. Since the earlier *PKPdf* arrival is strongly attenuated in the high frequency, as shown in Figure 2, the scattered *PK*Pbc* energy forms the first notable arrival.

We summarize that (a) scattering of core phases in the lower mantle is a commonly accepted process as confirmed for example by the *PKPdf* precursor at $\Delta < 145^\circ$. (b) Diffraction at the ICB is an unlikely mechanism because of the high frequencies used here (c) in simulations of energy propagation considering scattering in the lower mantle predict the arrival of energy that is in qualitative agreement with the observation of the *PKPab* precursor (cf., Figures 1–3). Furthermore (d) the curvature of the onset time curve of the *PKPab* precursor makes an origin at the ICB unlikely. These ideas strongly support the hypothesis that the observed *PKPab* precursor at $\Delta > 155^\circ$ is a consequence of the same process that causes the well-known *PKP* precursor at $\Delta < 145^\circ$ —the scattering in the heterogeneous lower mantle.

4. Local Sensitivity of the *PKPab* Precursor to Scattering

Waves scattered in the deep Earth provide means to investigate the structure of the lower mantle at a spatial scale below the resolution limits of seismic tomography. The *PKPab* precursor offers a new opportunity for this. Here, we investigate the spatial sensitivity of this signal. We use the theory of Margerin et al. (2016) to derive an intensity sensitivity kernel, which describes the sensitivity of the seismogram envelope to a local

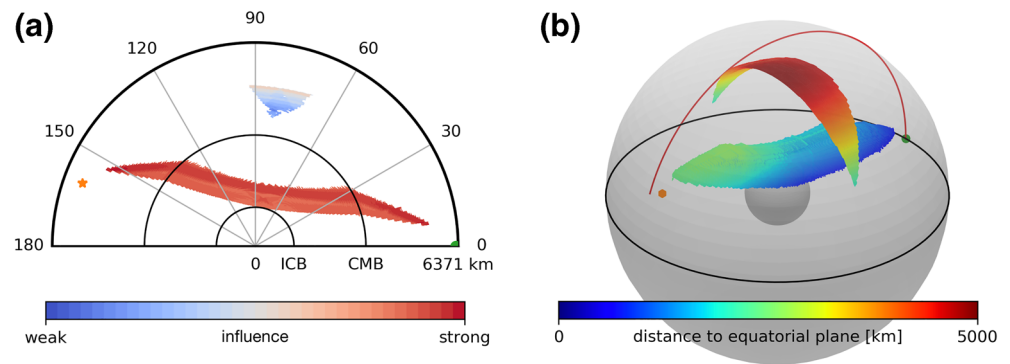


Figure 4. Volume of sensitivity for an arrival at 1,155 s lapse time and epicentral distance of $\Delta = 160^\circ$. Orange star and green circle indicate locations of source and receiver, respectively. (a) Cross section in the great-circle plane of source and receiver with warm colors indicating high sensitivity of the arrival to scattering. CMB and ICB are indicated. (b) 3D representation of the volume of sensitivity with color indicating distance to the equatorial plane. Two distinct regions of sensitivity exist. One is draped on the inner core along the *PKPbc* path. Due to the high *PKP* amplitudes, heterogeneity in this volume has a strong influence on amplitudes of the precursor. Another sickle-shaped region of sensitivity that allows for large deviations from the great circle is formed by scattering of *P* waves in the mantle. Heterogeneity in this region, however, has less influence on the amplitude of the *PKPab* precursor than in the elongated region that extends through the deep Earth (cf., Figure 4(a)). CMB, core-mantle boundary; ICB, inner core boundary.

increase of scattering strength. We simplify the treatment in three ways. (a) Wave propagation through the inner core is blocked. Since we observe that *PKPdf* waves vanish in the 4–8 Hz frequency range (cf., Figures 2b, 3, S2, and S3), waves that propagate through the inner core cannot contribute to the scattered arrival either. Scattering within the inner core would generate *PKPdf* coda rather than a separate phase that is disconnected from the *PKPdf* arrival. (b) We assume that scattering leading to the *PKPab* precursor is isotropic, which simplifies the treatment of scattering angles. Increased probability of forward scattering would reduce the probability of scattering close to either source or receiver. (c) The scattering process is restricted to a single scattering of *P* waves because *S* wave propagation is highly unlikely for the short travel time of the *PKPab* precursor.

Under the assumptions made, we can calculate the volume in which scattering can contribute to the observed *PKPab* precursor by convolution of the forward and backward *P* wave intensity. These intensities can be obtained by radiative transfer simulations, as described in Text S1 for excitation at the location of the earthquake (forward simulation) and the location of the receiver (backward simulation). The sensitivity finally describes the probability of a wave packet that arrives in a particular time–distance window to have traveled from the source to a particular location in space where scattering occurred, and then continued to the receiver location.

Figure 4(a) shows a cross section through the sensitivity kernel in the great-circle plane for an epicentral distance of $\Delta = 160^\circ$ and a lapse time of 1,155 s, which is within the time–distance window of the *PKPab* precursor. It describes the influence of heterogeneity (i.e., the possibility for wave scattering) on the amplitude of the *PKPab* precursor. Regions, where this probability is high, have a strong influence on the precursor amplitude. If this probability is low at some location, the influence is weak because it is unlikely that a wave arriving in the time–distance window was scattered there. Zero influence means that it is impossible for wave energy to arrive in the time–distance window of the *PKPab* precursor even if it is scattered there.

High sensitivity is located along the *PKPbc* path through the outer core and lower mantle. In this narrow volume, waves are scattered mostly in the forward direction meaning that small perturbations of the propagation direction of *PKPbc* waves can generate the *PKPab* precursor at 1,155 s at 160° distance. Due to the high amplitude of the *PKP* phase, the influence of this region on the *PKPab* precursor amplitude is high as indicated by the color in Figure 4(a). Another patch of sensitivity is located in the midmantle. It indicates that scattering of *P* waves in the midmantle allows waves to travel around the slow outer core and still carry energy to a receiver in the time–distance window of the *PKPab* precursor. However, considering the smaller

amplitudes of the participating waves, there is a low probability that the scattering in this region contributes to the observed signal—resulting in a weak influence of this region on the precursor.

Since scattering allows for off great-circle path propagation, the sensitivity has a significant 3D component, as illustrated in Figure 4(b). The volume with the strong influence on the *PKPab* precursor that extends through the deep Earth is draped on the inner core and shows small deviations from the great-circle plane. The region of *P* wave scattering in the midmantle forms a sickle-shaped volume of sensitivity, perpendicular to the great-circle plane. Energy in the *PKPab* precursor window that was scattered in the mantle can, therefore, arrive with significant deviations from the great-circle direction.

5. Discussion

Using numerical simulations, we show that scattering in the lower mantle results in the arrival of scattered energy before the *PKPab* phase at $\Delta > 155^\circ$. This energy arrives after *PKPdf*. In the high-frequency band between 4 Hz and 8 Hz, waves do not propagate through the inner core on the path between South America and Japan due to high intrinsic or scattering attenuation in the inner core. This vanishing of the *PKPdf* energy makes the *PKPab* precursor the first notable arrival on seismograms recorded in this distance range, which can be readily observed in individual records of deep earthquakes. We speculate that the *PKPab* precursory signal is also present at lower frequencies where it is masked by the earlier *PKPdf* arrival and its coda. For the outer core and the mantle, our observations of 6 Hz core phases imply the need for high *Q* at this frequency range.

The origin of the *PKPab* precursor has been discussed earlier. A number of articles discussed the *PKP* – *C_{diff}* phase that should result from the diffraction of compressional waves around the inner core along the ICB. Nakanishi (1990) present observations of 2.5–3.3 Hz *PKP* – *C_{diff}* waves in the distance range $152^\circ < \Delta < 157^\circ$. From the complex, long-lasting waveforms, their earliest arrival, and their high slowness, Nakanishi (1990) concluded that scattering at the base of the upper mantle around 660 km depth is more likely to generate these arrivals than ICB diffraction. Tanaka (2005) investigated *PKP* – *C_{diff}* coda using short-period seismic arrays and found slowness ranging between 1 s/° and 5 s/° extending through the whole range covered by *PKPab* and *PKPbc* waves. Scattering at the CMB was invoked as an alternative origin of the *PKP* – *C_{diff}* coda signal, since the slowness of waves scattered close to the c-cusp is too close to that of *PKP* – *C_{diff}* waves to be separated by the arrays. These early works are thus in agreement with our interpretation of the *PKPab* precursor as scattered *PKPbc* with a likely location of the scattering close to the CMB.

Adam and Romanowicz (2015) report on a scattered phase that arrives 5–20 s after the *PKPbc* or *PKP* – *C_{diff}* phases which they call *M*-phase. Adam and Romanowicz (2015) use coherent stacking of 1 Hz signals within distance ranges up to 10° and conclude that the scattered *M*-phase originates at the ICB. Scattering at the CMB was ruled out because the *M*-phase appears as an isolated phase in the phase weighted stack with a slowness between 0.7 s/° and 1.6 s/°. This slowness is too low for *PKPbc* waves scattered at the CMB beyond 160° distance. This finding appears to contradict our interpretation. However, first the 1 Hz frequency range differs from our observation and second the argument that Adam and Romanowicz (2015) use to rule out the possibility of *PKPbc* scattering close to the CMB is strongly based on the limitation of the slowness range to 1.6 s/° maximum. This constraint is derived under the assumption of distance independent slowness even though it is not shown that the *M*-phase at $\Delta > 160^\circ$ has a slowness below 1.6 s/°. The fact that the *M*-phase appears as an isolated phase is enforced by the phase weighted stacking and does not exclude the actual presence of an extended wave train originating from waves with a significant spread of slowness and back azimuth.

Thus, we think that our interpretation of the *PKPab* precursor, as scattered *PKPbc* waves are compatible with earlier studies. Other effects like diffraction or propagation in thin heterogeneous low-velocity layers at ICB and CMB might additionally affect high-frequency *PKP* waves and cannot be ruled out. But they are not required to explain the present observations. The discussed *PKP* – *C_{diff}* coda, as well as the *M*-phase, may be interpreted as a signal with the same origin as the *PKPab* precursor. Since the heterogeneity at *D''* is widely accepted, it should be taken into account in any interpretation of signals that might have passed through *D''*. This concerns all investigations of the inner core. The difference in coda decay between *PcP* and *PKiKP*

coda at small distances, for example, should not be interpreted without considering the effect of the twofold *PKiKP* transmissions through D'' which can significantly alter the shape of the coda.

The possibility to observe the *PKPab* precursor at $\Delta > 155^\circ$ requires strong attenuation of the earlier arriving *PKPdf* waves that pass through the inner core. Longitudinal variations of *PKiKP* versus *PKPdf* travel time and amplitude differences indicate hemispherical asymmetry of inner core attenuation (Monnereau et al., 2010). This will likely influence the observability of the *PKPab* precursor. The *PKPab* precursor in locations where it can be observed can increase the lateral resolution of *PKP*-based CMB studies. Combined with observations of the *PKPdf* precursor, it allows using earthquakes from a much wider distance range. The observation of scattered waves at the exceptionally high frequencies used here provides means for the investigation of heterogeneity in the deep Earth at a length scale of the order of a kilometer or below.

As indicated by the elongated shape of the sensitivity kernel in Figure 4, the vertical resolution of the scattering location is relatively poor. Since the required deviation of the propagation direction (scattering angle) is small, the scattering can happen almost anywhere between the source and receiver. However, it is known from array analysis of the *PKPdf* precursor (e.g., Thomas et al., 1999) that the most likely location of scattering is D'' . Considering that scattering cannot occur in the outer core the *PK*Pbc* onset time is the earliest possible time for the arrival of scattered energy and Figures 2 and 3 clearly show that there is no earlier arrival. As heterogeneity shallower in the mantle causes later arrivals, the emergent increase of *PKPab* precursor energy might thus indicate that scattering is not confined to the CMB but might occur in a larger part of the lower mantle.

The theoretical possibility of propagating seismic energy in the time–distance window of the *PKPab* precursor by *P*P* scattering in the midmantle (cf., Figure 4) is challenging to test because of the much stronger *PKP* phases. However, for scattering deeper in the mantle, the *P*P* scattered waves can arrive prior to any scattered core phase and could be used to investigate scattering above D'' .

6. Conclusion

We show that the frequency range for investigation of the deep Earth with teleseismic waves can be extended toward frequencies of several Hertz. The attenuation of high-frequency waves in the inner core allows for the observation of scattered *PKPbc* waves as *PKPab* precursor in the shadow of the inner core. Without this attenuation, the *PKPab* precursor would be masked by the *PKPdf* coda (which is likely the case at lower frequencies). This situation is similar to the *PKPdf* precursor that can only be so clearly observed as the first arriving phase because the low-velocity core deviates the *P* phase—thereby creating the (outer) core shadow.

We calculate the sensitivity kernels of the *PKPab* precursor for heterogeneity using elastic radiative transfer simulations. The kernels describe the Earth's region in which scattering would contribute to seismic energy's arrival in a given time–distance window. Scattering in D'' that causes the *PKPdf* precursor at $\Delta < 145^\circ$ is also the most likely mechanism causing the *PKPab* precursor at $\Delta > 155^\circ$. Combining these sensitivities kernels with observations of scattered energy from *PKPab* and *PKPdf* precursors will improve the imaging and characterization of heterogeneity in the deep Earth.

Data Availability Statement

Data from Japan (NIED, 2019) were kindly provided by the National Research Institute for Earth Science and Disaster Resilience and are available at www.hinet.bosai.go.jp. Data from Brazil were kindly provided by the Brazilian seismographic network (RSBR) and the participating institutions. They are available from www.rsbr.gov.br with details about access given in Bianchi et al. (2018).

Acknowledgments

K. Bataille acknowledges support from DAAD for his stay in Potsdam.

References

- Adam, J.-C., & Romanowicz, B. (2015). Global scale observations of scattered energy near the inner-core boundary: Seismic constraints on the base of the outer-core. *Physics of the Earth and Planetary Interiors*, 245, 103–116. <https://doi.org/10.1016/j.pepi.2015.06.005>
- Aki, K., & Chouet, B. (1975). Origin of coda waves: Source, attenuation, and scattering effects. *Journal of Geophysical Research*, 80(23), 3322–3342. <https://doi.org/10.1029/JB080i023p03322>

- Bataille, K., & Lund, F. (1996). Strong scattering of short-period seismic waves by the core–mantle boundary and the P-diffracted wave. *Geophysical Research Letters*, 23(18), 2413–2416. <https://doi.org/10.1029/96GL02225>
- Bianchi, M. B., Assumpção, M., Rocha, M. P., Carvalho, J. M., Azevedo, P. A., Fontes, S. L., et al. (2018). The Brazilian seismographic network (RSBR): Improving seismic monitoring in Brazil. *Seismological Research Letters*, 89(2A), 452–457. <https://doi.org/10.1785/0220170227>
- Burke, K., Steinberger, B., Torsvik, T. H., & Smethurst, M. A. (2008). Plume generation zones at the margins of large low shear velocity provinces on the core–mantle boundary. *Earth and Planetary Science Letters*, 265(1–2), 49–60. <https://doi.org/10.1016/j.epsl.2007.09.042>
- Chang, A. C., & Cleary, J. R. (1978). Precursors to PKKP. *Bulletin of the Seismological Society of America*, 68(4), 1059–1079. <https://doi.org/10.1017/CBO9781107415324.004>
- Chang, A. C., & Cleary, J. R. (1981). Scattered PKKP: Further evidence for scattering at a rough core–mantle boundary. *Physics of the Earth and Planetary Interiors*, 24(1), 15–29. [https://doi.org/10.1016/0031-9201\(81\)90075-3](https://doi.org/10.1016/0031-9201(81)90075-3)
- Earle, P. S., & Shearer, P. M. (1997). Observations of PKKP precursors used to estimate small-scale topography on the core–mantle boundary. *Science*, 277(5326), 667–670. <https://doi.org/10.1126/science.277.5326.667>
- Earle, P. S., & Shearer, P. M. (2001). Distribution of fine-scale mantle heterogeneity from observations of Pdiff coda. *Bulletin of the Seismological Society of America*, 91(6), 1875–1881.
- Euler, G. G., & Wysession, M. E. (2017). Geographic variations in lowermost mantle structure from the ray parameters and decay constants of core-diffracted waves. *Journal of Geophysical Research: Solid Earth*, 122, 5369–5394. <https://doi.org/10.1002/2017JB013930>
- French, S. W., & Romanowicz, B. (2015). Broad plumes rooted at the base of the Earth's mantle beneath major hotspots. *Nature*, 525(7567), 95–99. <https://doi.org/10.1038/nature14876>
- Frost, D. A., & Rost, S. (2014). The P-wave boundary of the large-low shear velocity province beneath the Pacific. *Earth and Planetary Science Letters*, 403, 380–392. <https://doi.org/10.1016/j.epsl.2014.06.046>
- Gaebler, P. J., Sens-Schönfelder, C., & Korn, M. (2015). The influence of crustal scattering on translational and rotational motions in regional and teleseismic coda waves. *Geophysical Journal International*, 201, 355–371. <https://doi.org/10.1093/gji/ggv006>
- Gassner, A., Thomas, C., Krüger, F., & Weber, M. (2015). Probing the core–mantle boundary beneath Europe and Western Eurasia: A detailed study using PcP. *Physics of the Earth and Planetary Interiors*, 246, 9–24. <https://doi.org/10.1016/j.pepi.2015.06.007>
- Haddon, R. A. W., & Cleary, J. R. (1974). Evidence for scattering of seismic PKP waves near the mantle–core boundary. *Physics of the Earth and Planetary Interiors*, 8(3), 211–234. [https://doi.org/10.1016/0031-9201\(74\)90088-0](https://doi.org/10.1016/0031-9201(74)90088-0)
- Hansen, S. E., Carson, S. E., Garnero, E. J., Rost, S., & Yu, S. (2020). Investigating ultra-low velocity zones in the southern hemisphere using an Antarctic dataset. *Earth and Planetary Science Letters*, 536, 116142. <https://doi.org/10.1016/j.epsl.2020.116142>
- Hedlin, M. A. H., Shearer, P. M., & Earle, P. S. (1997). Seismic evidence for small-scale heterogeneity throughout the Earth's mantle. *Nature*, 387(6629), 145–150. <https://doi.org/10.1038/387145a0>
- Kennett, B. L., Engdahl, E. R., & Buland, R. (1995). Constraints on seismic velocities in the Earth from traveltimes. *Geophysical Journal International*, 122(1), 108–124. <https://doi.org/10.1111/j.1365-246X.1995.tb03540.x>
- Kustowski, B., Ekström, G., & Dziewoński, A. M. (2008). Anisotropic shear-wave velocity structure of the Earth's mantle: A global model. *Journal of Geophysical Research*, 113, B06306. <https://doi.org/10.1029/2007JB005169>
- Labrosse, S. (2014). Thermal evolution of the core with a high thermal conductivity. *Physics of the Earth and Planetary Interiors*, 247, 36–55. <https://doi.org/10.1016/j.pepi.2015.02.002>
- Lay, T., & Garnero, E. J. (2011). Deep mantle seismic modeling and imaging. *Annual Review of Earth and Planetary Sciences*, 39(1), 91–123. <https://doi.org/10.1146/annurev-earth-040610-133354>
- Margerin, L., Planès, T., Mayor, J., & Calvet, M. (2016). Sensitivity kernels for coda-wave interferometry and scattering tomography: Theory and numerical evaluation in two-dimensional anisotropically scattering media. *Geophysical Journal International*, 204(1), 650–666. <https://doi.org/10.1093/gji/ggv470>
- McNamara, A. K. (2019). A review of large low shear velocity provinces and ultra low velocity zones. *Tectonophysics*, 760, 199–220. <https://doi.org/10.1016/j.tecto.2018.04.015>
- Monnereau, M., Calvet, M., Margerin, L., & Souriau, A. (2010). Lopsided growth of Earth's inner core. *Science*, 328(5981), 1014–1017. <https://doi.org/10.1126/science.1186212>
- Montagner, J. P., & Kennett, B. L. (1996). How to reconcile body-wave and normal-mode reference earth models. *Geophysical Journal International*, 125(1), 229–248. <https://doi.org/10.1111/j.1365-246X.1996.tb06548.x>
- Nakanishi, I. (1990). High-frequency waves following PKP-CDIFF at distances greater than 155°. *Geophysical Research Letters*, 17(5), 639–642.
- NIED. (2019). *NIED Hi-net*. Japan: National Research Institute for Earth Science and Disaster Resilience. <https://doi.org/10.17598/NIED.0003>
- Obara, K., Kasahara, K., Hori, S., & Okada, Y. (2005). A densely distributed high-sensitivity seismograph network in Japan: Hi-net by National Research Institute for Earth Science and Disaster Prevention. *Review of Scientific Instruments*, 76(2005), 021301. <https://doi.org/10.1063/1.1854197>
- Obara, K., & Sato, H. (1995). Regional differences of random inhomogeneities around the volcanic front in the Kanto-Tokai area, Japan, revealed from the broadening of S wave seismogram envelopes. *Journal of Geophysical Research*, 100(94), 2103–2121. <https://doi.org/10.1029/94JB02644>
- Okada, Y., Kasahara, K., Hori, S., Obara, K., Sekiguchi, S., Fujiwara, H., & Yamamoto, A. (2004). Recent progress of seismic observation networks in Japan—Hi-net, F-net, K-net and KiK-net. *Earth, Planets and Space*, 56(XV–XXVIII). <https://doi.org/10.1088/1742-6596/433/1/012039>
- Olson, P. (2016). Mantle control of the geodynamo: Consequences of top-down regulation. *Geochemistry, Geophysics, Geosystems*, 17, 1935–1956. <https://doi.org/10.1002/2016GC006334>
- Pacheco, C., & Snieder, R. (2005). Time-lapse travel time change of multiply scattered acoustic waves. *Journal of the Acoustical Society of America*, 118(3), 1300. <https://doi.org/10.1121/1.2000827>
- Ritsema, J., Deuss, A., Van Heijst, H. J., & Woodhouse, J. H. (2011). S40RTS: A degree-40 shear-velocity model for the mantle from new Rayleigh wave dispersion, teleseismic traveltimes and normal-mode splitting function measurements. *Geophysical Journal International*, 184(3), 1223–1236. <https://doi.org/10.1111/j.1365-246X.2010.04884.x>
- Schubert, B. S., Bunge, H. P., & Ritsema, J. (2009). Tomographic filtering of high-resolution mantle circulation models: Can seismic heterogeneity be explained by temperature alone? *Geochemistry, Geophysics, Geosystems*, 10, Q05W03. <https://doi.org/10.1029/2009GC002401>
- Sens-Schönfelder, C., Margerin, L., & Campillo, M. (2009). Laterally heterogeneous scattering explains Lg blockage in the Pyrenees. *Journal of Geophysical Research*, 114, B07309. <https://doi.org/10.1029/2008JB006107>

- Shearer, P. M. (2015). Deep Earth structure—Seismic scattering in the deep Earth. In *Treatise on Geophysics* (Vol. 1, 2nd ed.). Elsevier B.V. <https://doi.org/10.1016/B978-0-444-53802-4.00018-X>
- Shen, Z., Ni, S., Wu, W., & Sun, D. (2016). Short period ScP phase amplitude calculations for core–mantle boundary with intermediate scale topography. *Physics of the Earth and Planetary Interiors*, 253, 64–73. <https://doi.org/10.1016/j.pepi.2016.02.002>
- Sun, D., Helmberger, D. V., Jackson, J. M., Clayton, R. W., & Bower, D. J. (2013). Rolling hills on the core–mantle boundary. *Earth and Planetary Science Letters*, 361, 333–342. <https://doi.org/10.1016/j.epsl.2012.10.027>
- Tackley, P. J. (2012). Dynamics and evolution of the deep mantle resulting from thermal, chemical, phase and melting effects. *Earth-Science Reviews*, 110(1–4), 1–25. <https://doi.org/10.1016/j.earscirev.2011.10.001>
- Takeuchi, N. (2016). Differential Monte Carlo method for computing seismogram envelopes and their partial derivatives. *Journal of Geophysical Research: Solid Earth*, 121, 3428–3444. <https://doi.org/10.1002/2015JB012661>
- Tanaka, S. (2005). Characteristics of PKP-Cdiff coda revealed by small-aperture seismic arrays: Implications for the study of the inner core boundary. *Physics of the Earth and Planetary Interiors*, 153(1–3), 49–60. <https://doi.org/10.1016/j.pepi.2005.05.007>
- Thomas, C., Weber, M., Wicks, C. W., & Scherbaum, F. (1999). Small scatterers in the lower mantle observed at German broadband arrays. *Journal of Geophysical Research*, 104(B7), 15073–15088. <https://doi.org/10.1029/1999JB900128>
- Trabant, C., Hutko, A. R., Bahavar, M., Karstens, R., Ahern, T., & Aster, R. (2012). Data products at the IRIS DMC: Stepping stones for research and other applications. *Seismological Research Letters*, 83(5), 846–854. <https://doi.org/10.1785/0220120032>
- Wang, Y., & Wen, L. (2004). Mapping the geometry and geographic distribution of a very low velocity province at the base of the Earth's mantle. *Journal of Geophysical Research*, 109, B10305–18. <https://doi.org/10.1029/2003JB002674>
- Wu, W., Ni, S., & Shen, Z. (2014). Constraining the short scale core–mantle boundary topography beneath Kenai Peninsula (Alaska) with amplitudes of core-reflected PcP wave. *Physics of the Earth and Planetary Interiors*, 236, 60–68. <https://doi.org/10.1016/j.pepi.2014.09.001>
- Yu, S., & Garnero, E. J. (2018). Ultralow velocity zone locations: A global assessment. *Geochemistry, Geophysics, Geosystems*, 19, 396–414. <https://doi.org/10.1002/2017GC007281>
- Zou, Z., Koper, K. D., & Cormier, V. F. (2008). The structure of the base of the outer core inferred from seismic waves diffracted around the inner core. *Journal of Geophysical Research*, 113, B05314. <https://doi.org/10.1029/2007JB005316>